

# Sensitivity of the Climate Response to the Altitude of Black Carbon in the Northern Subtropics in an Aquaplanet GCM

HANJUN KIM AND SARAH M. KANG

*School of Urban and Environmental Engineering, Ulsan National Institute of Science and Technology, Ulsan, South Korea*

YEN-TING HWANG

*Department of Atmospheric Sciences, National Taiwan University, Taipei, Taiwan*

YOUNG-MIN YANG

*International Pacific Research Center, University of Hawai'i at Mānoa, Honolulu, Hawaii*

(Manuscript received 13 January 2015, in final form 25 April 2015)

## ABSTRACT

This study explores the dependence of the climate response on the altitude of black carbon in the northern subtropics by employing an atmospheric general circulation model coupled to an aquaplanet mixed layer ocean, with a focus on the pattern changes in the temperature, hydrological cycle, and large-scale circulation. Black carbon added below or within the subtropical low-level clouds tends to suppress convection, which reduces the low cloud amount, resulting in a positive cloud radiative forcing. The warmer northern subtropics then induce a northward shift of the intertropical convergence zone (ITCZ) and a poleward expansion of the descending branch of the northern Hadley cell. As the black carbon-induced local warming is amplified by clouds and is advected by the anomalous Hadley circulation, the entire globe gets warmer. In contrast, black carbon added near the surface increases the buoyancy of air parcels to enhance convection, leading to an increase in the subtropical low cloud amount and a negative cloud radiative forcing. The temperature increase remains local to where black carbon is added and elsewhere decreases, so that the ITCZ is shifted southward and the descending branch of the northern Hadley cell contracts equatorward. Consistent with previous studies, the authors demonstrate that the climate response to black carbon is highly sensitive to the vertical distribution of black carbon relative to clouds; hence, models have to accurately compute the vertical transport of black carbon to enhance their skill in simulating the climatic effects of black carbon.

## 1. Introduction

Black carbon (BC) is a typical absorbing aerosol in that it directly absorbs shortwave radiation, exerting a net positive radiative forcing at the top of the atmosphere (Hansen et al. 2005). Hence, BC is generally considered a strong contributor to global warming together with greenhouse gases (Ramanathan and Carmichael 2008). However, BC is differentiated from greenhouse gases that absorb and emit longwave radiation as it simultaneously warms the atmosphere and cools the surface by attenuating the amount of solar

radiation reaching the surface. Thus, BC can effectively alter the atmospheric static stability and influence circulation as well as the formation and distribution of clouds and the hydrological cycle (Ramanathan et al. 2001; Johnson et al. 2004; Ming et al. 2010; Wang 2013). This aerosol–cloud feedback without any cloud microphysical processes is called the semidirect effect, apart from the direct effect that refers to the mechanism by which the aerosols absorb or reflect incoming solar radiation.

A number of previous studies have demonstrated that the climatic impacts of BC depend on the altitude of BC by performing general circulation model (GCM) experiments with a globally uniform increase in BC at different vertical levels (e.g., Cook and Highwood 2004; Hansen et al. 2005; Persad et al. 2012; Ban-Weiss et al. 2012). For example, it is generally thought that

---

*Corresponding author address:* Sarah M. Kang, School of Urban and Environmental Engineering, Ulsan National Institute of Science and Technology, UNIST-gil 50, Ulsan 689-798, South Korea.  
E-mail: skang@unist.ac.kr

additional BC suppresses the hydrological cycle because of stronger atmospheric heating, but BC near the surface is shown to decrease the vertical stability and acts to increase precipitation (Ming et al. 2010; Ban-Weiss et al. 2012). Moreover, whether BC increases or decreases cloud cover is shown to depend on the altitude of BC relative to the cloud and the cloud type (Koch and Del Genio 2010; Sakaeda et al. 2011). Large-eddy simulations also show that the vertical distribution of BC is crucial to determining the response of low cloud amount (Johnson et al. 2004; Feingold et al. 2005). This contrasting effect of BC on clouds results in a large sensitivity in the degree of surface warming as the altitude of additional BC is varied (Ban-Weiss et al. 2012). Because the vertical profile of BC in the atmosphere is generally poorly known and because of the uncertainty in the parameterized cloud field, the estimate of the semidirect effect is highly uncertain (Bond et al. 2013).

To examine the climate response to the altitude of BC, previous studies mostly performed experiments in which the model climate is perturbed by injecting a globally uniform layer of BC at different levels. There is, however, substantial geographical inhomogeneity in the global distribution of BC emissions with a peak in African savannah, India, and southern China (Bond et al. 2004). The future emission scenarios project similar regional variability (see Fig. 2.13 in UNEP/WMO 2011). Hence, in this study, we investigate the sensitivity of global climate response to the altitude of BC in the subtropical subsidence region in the Northern Hemisphere. To help elucidate fundamental mechanisms, an idealized experimental setup is utilized in which an atmospheric GCM coupled to aquaplanet mixed layer ocean is employed. Other previous studies tend to focus on the global-mean changes, but here we are particularly interested in the changes in temperature patterns, hydrological cycle, and large-scale circulation.

## 2. Methodology

We employ the atmospheric GCM, Atmosphere Model version 2.1 (AM2.1), developed at the Geophysical Fluid Dynamics Laboratory (GFDL) that is coupled to a 2.4-m aquaplanet mixed layer ocean to allow sea surface temperatures (SSTs) to freely evolve (Anderson et al. 2004). The model has a horizontal resolution of  $2^\circ$  latitude  $\times$   $2.5^\circ$  longitude with 24 vertical levels. Insolation is prescribed to the annual-mean profile. The control climate with no aerosol is perturbed by inserting 200 Gg of BC in the northern subtropics at a specific  $\sigma$  layer (Fig. 1). Since observed BC concentrations are primarily located in the lower troposphere rather than at high altitudes and are concentrated in the

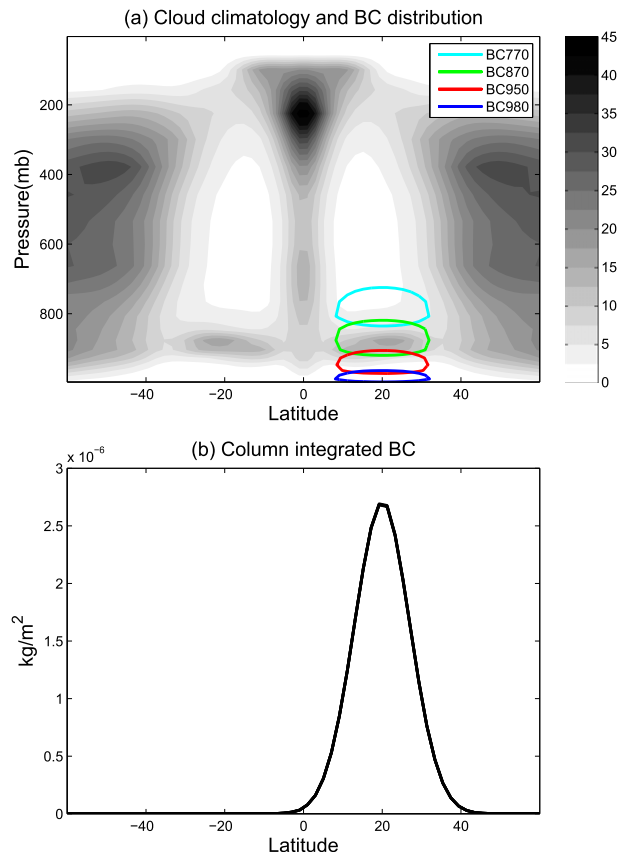


FIG. 1. (a) The zonal-mean cloud fraction in the control experiment (shading) and the location of prescribed BC in BC770 (cyan), BC870 (green), BC950 (red), and BC980 (blue). (b) The column integrated concentration ( $10^{-6} \text{ kg m}^{-2}$ ) of prescribed BC in all cases.

northern subtropics (Ramanathan et al. 2007), we place the BC burden below 700 hPa, with a Gaussian distribution in latitude centered at  $20^\circ\text{N}$ . Since the relative altitude of BC to clouds is reported to be critical for determining the climate response (Koch and Del Genio 2010), the same BC burden is added at four different layers: near the surface (980 hPa) and below (950 hPa), within (870 hPa), and above (770 hPa) the climatological mean subtropical low clouds in the control climate (Fig. 1a). Each experiment is indexed by the pressure level at which the maximum BC concentration occurs. In a realistic case, BC is not confined to a single layer, so we also performed experiments where BC is prescribed at two adjacent  $\sigma$  layers. The result is close to the linear summation of the response of two experiments where BC is prescribed at a single layer (not shown). The model includes direct and semidirect aerosol effects but excludes indirect effects (aerosol–cloud microphysics coupling). Optical properties for BC are based on satellite observation of Haywood et al. (1999).

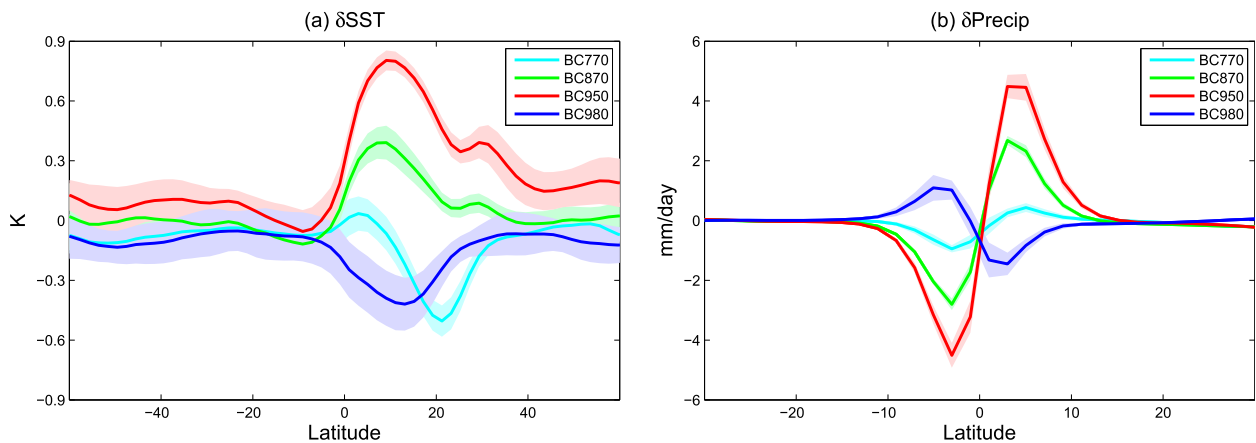


FIG. 2. Solid lines indicate the ensemble-mean of zonal-mean change in (a) SST (K) and (b) precipitation ( $\text{mm day}^{-1}$ ) in BC770 (cyan), BC870 (green), BC950 (red), and BC980 (blue). Shading represents plus or minus one standard deviation of six ensemble members.

The control experiment is run for 60 years and the first 2 years are discarded as spinup. Each BC added experiment consists of six ensemble members where the BC burden is abruptly added at a different day after the spinup period of the control experiment. Each member is run for 10 years and the last 8-yr average is used for the analysis. Results presented are based on the ensemble mean. The difference between the BC added and the control experiments will be denoted with  $\delta$ .

To help interpret the cloud response in the mixed layer experiments, the same experiments are performed in which cloud radiative feedback is suppressed. A 1-yr time series of 3-hourly cloud water mixing ratio, cloud ice mixing ratio, and fractional cloud from the control experiment are inserted into both the control and the perturbed BC experiments. More details on fixed cloud experiments can be found in Kang et al. (2008). The fixed cloud experiments will be denoted with the “fixcld” subscript. Furthermore, to understand the fast response and separate out the SST-induced response, the same experiments are performed with the SSTs specified to the control climatology. The fixed SST experiments will be denoted with the “fixsst” subscript. Results presented for the experiments with fixed cloud or SST are averages of the last 18 years of the 20-yr runs.

### 3. Results

Figure 2 shows the zonal-mean changes in SST (Fig. 2a) and precipitation (Fig. 2b) as BC is added at different layers in the northern subtropics. Although the solar absorption by BC warms the level at which BC is added (refer to Fig. 6), the surface temperature response depends greatly on the vertical position of BC. In the northern tropics, the largest surface warming occurs in

case BC950, with a weaker warming in BC870. In the other two cases, the surface is significantly cooled. Despite one model layer difference in the vertical level of prescribed BC, BC950 and BC980 exhibit the largest contrast, with responses opposite in sign. In all cases, the change in the global-mean precipitation is negligible but the pattern of tropical precipitation exhibits a substantial change with a clear latitudinal shift of the intertropical convergence zone (ITCZ). The ITCZ in BC950 is shifted northward the most, consistent with the largest surface warming in the northern tropics. Conversely, BC980 with surface cooling in the northern tropics exhibits a southward ITCZ shift. These zonal-mean analyses clearly demonstrate that the patterns of temperature and precipitation responses are highly sensitive to the vertical distribution of BC.

The SST response can be understood by considering the response of the net top-of-atmosphere (TOA) radiation budget composed of both longwave (LW) and shortwave (SW) fluxes ( $\delta R_{\text{TOA}}$ ; Fig. 3a), which is primarily determined by the response of cloud radiative forcing ( $\delta \text{CRF}$ , Fig. 3b), exclusively from changes in SW cloud reflection (not shown). For example, the largest northern subtropical warming in BC950 is consistent with the least SW cloud reflection. The hemispheric asymmetry in  $\delta R_{\text{TOA}}$  leads to a shift of the rising branch of the Hadley circulation (HC) toward the warmer hemisphere (see Fig. 5) in order to transport more energy toward the cooler hemisphere (Kang et al. 2008, 2009). The abundance of water vapor in the lower troposphere then causes an ITCZ shift toward the warmer hemisphere (Fig. 2b). The ITCZ shift results in the dipole pattern of  $\delta \text{CRF}$  in the deep tropics. The response of CRF in the fixed cloud experiments ( $\delta \text{CRF}_{\text{fixcld}}$ , Fig. 3c) is negligible except in the cases with BC added at

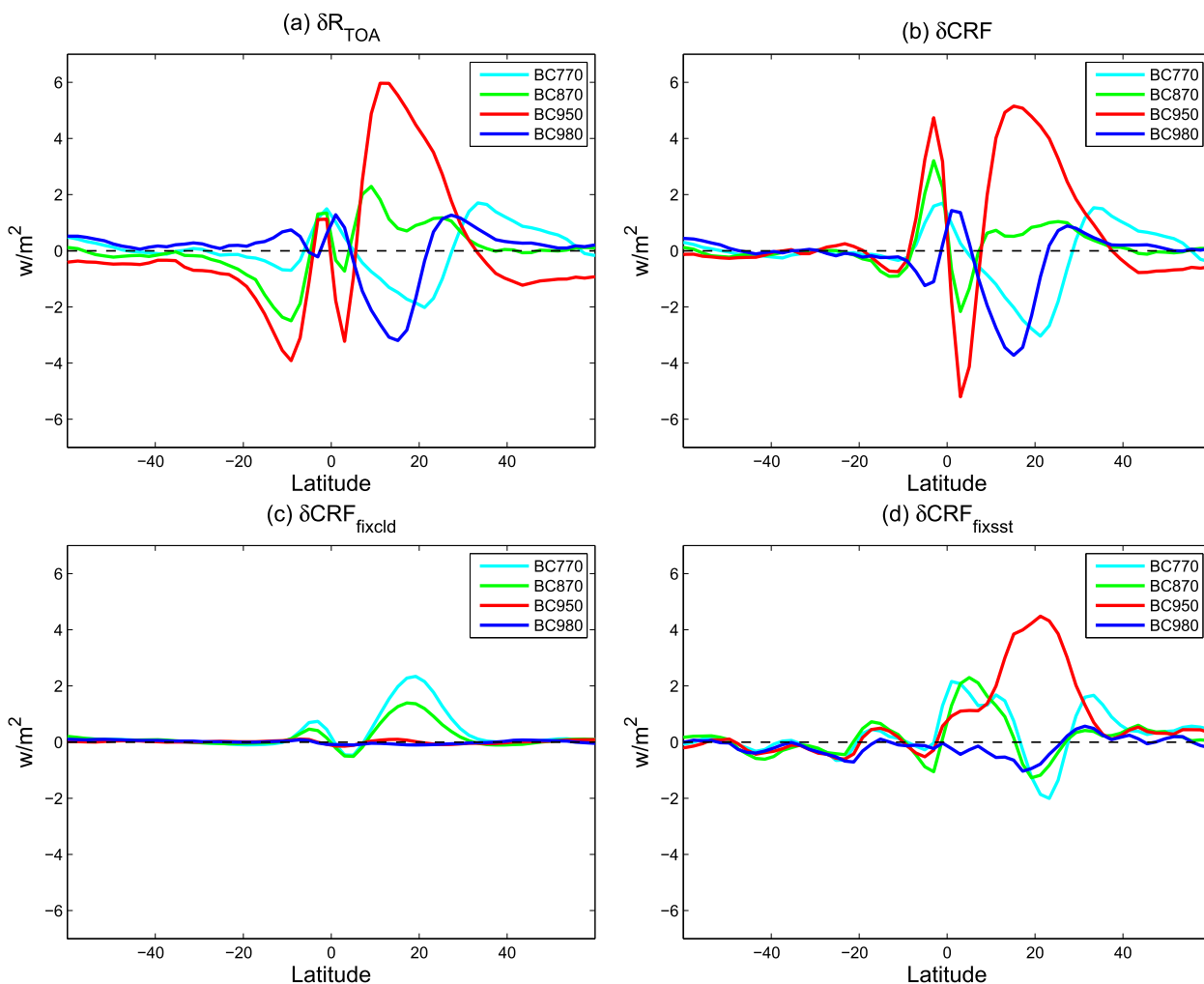


FIG. 3. (a) The zonal-mean change in net  $R_{\text{TOA}}$  ( $\text{W m}^{-2}$ ) in the mixed layer experiments. The zonal-mean change in CRF ( $\text{W m}^{-2}$ ) in the (b) mixed layer experiments, (c) fixed cloud experiments, and (d) fixed SST experiments: BC770 in cyan, BC870 in green, BC950 in red, and BC980 in blue.

the upper two layers, within and above the climatological cloud layer (BC870 and BC770). Since BC above the cloud layer absorbs upward radiation that is reflected by lower-level clouds (e.g., Ming et al. 2005; Zarzycki and Bond 2010; Persad et al. 2012), the CRF is positive even when cloud amounts are fixed. A comparison between  $\delta \text{CRF}$  (Fig. 3b) and  $\delta \text{CRF}_{\text{fixcl}}$  (Fig. 3c) indicates that most  $\delta \text{CRF}$  in the mixed layer experiments results from changes in the cloud amount, leading one to infer that the root cause for the large sensitivity in the climate response to BC altitude lies in the impact of BC on cloud amount. The similarity between the prescribed SST experiments (Fig. 3d) and the mixed layer experiments (Fig. 3b) in the northern subtropics suggests that cloud amount changes in the northern subtropics are the result of changes in local atmospheric stability rather than

changes in SST. In the deep tropics, the response of CRF in the fixed SST experiments ( $\delta \text{CRF}_{\text{fixsst}}$ ) is negligible because the ITCZ is locked at the latitude with maximum SST in the fixed SST cases.

Figure 4 explains the cause for the differing response of the cloud amount in the northern subtropics to the altitude of BC. We note that the change of cloud amount does not always correlate with changes in cloud SW optical depth. However, it is used as the measure of cloud optical properties because this is generally the case for warm clouds (Zelinka and Hartmann 2012), which are mainly discussed in the present study. In our control experiment, the base of subtropical clouds is located at approximately 950 hPa and the top at approximately 700 hPa, derived from the zero-crossing level of convective mass flux (not shown).

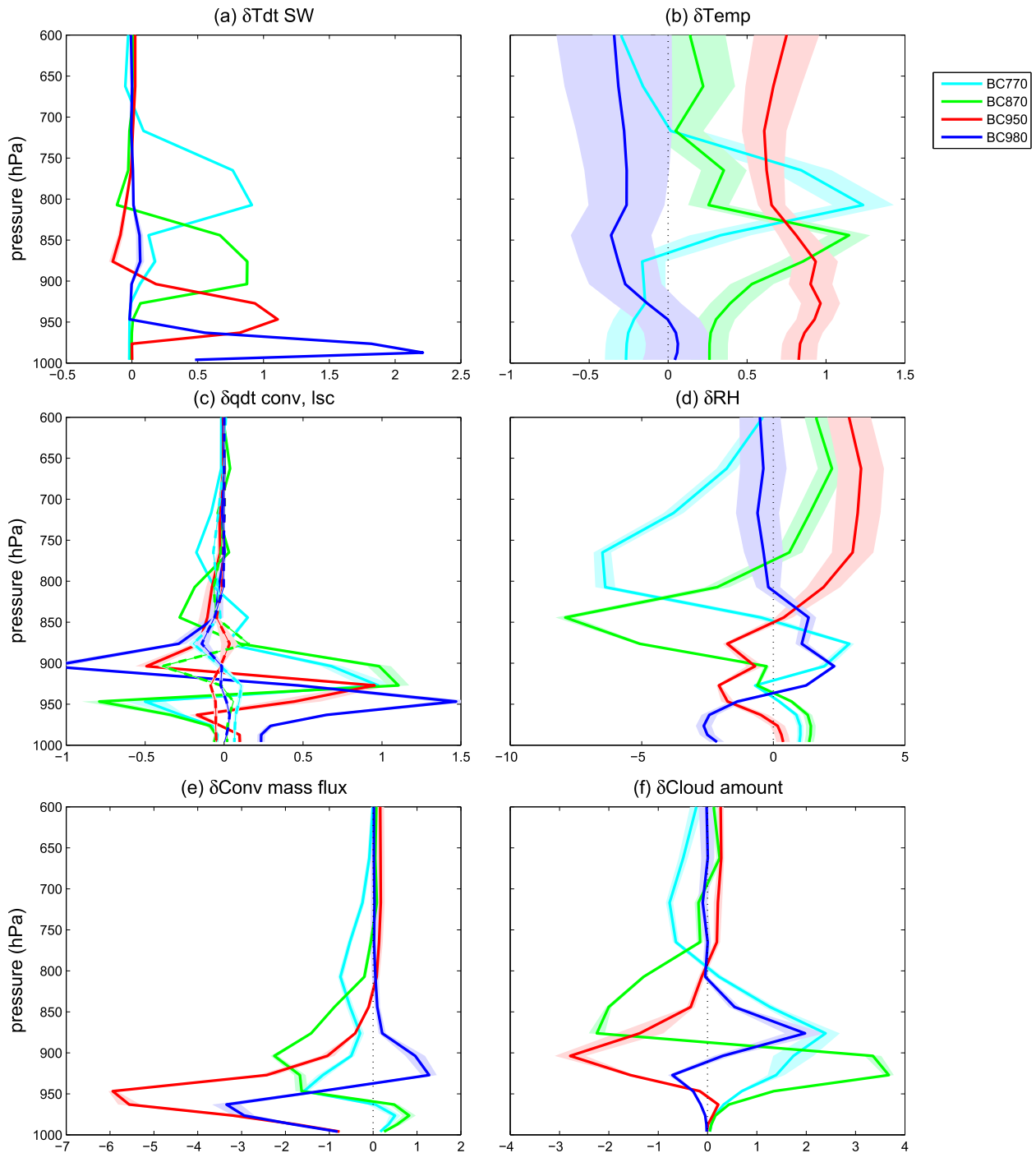


FIG. 4. Vertical distribution of the ensemble-mean averaged changes over  $10^{\circ}$ – $30^{\circ}$ N in (a) temperature tendencies ( $10^{-5} \text{ K s}^{-1}$ ) by shortwave heating, (b) temperature (K), (c) tendencies in water vapor mass mixing ratio ( $10^{-8} \text{ kg kg}^{-1} \text{ s}^{-1}$ ) by convection (solid) and large-scale condensation (dashed), (d) relative humidity (%), (e) convective mass flux ( $10^{-3} \text{ kg m}^{-2} \text{ s}^{-1}$ ), and (f) cloud amount (%): BC770 in cyan, BC870 in green, BC950 in red, and BC980 in blue. Shading represents plus or minus one standard deviation of six ensemble members.

In BC770, the BC-induced SW heating is maximized at 750–800 hPa (Fig. 4a), as is the vertical temperature anomaly (Fig. 4b). This tends to stabilize the lower troposphere and hinder moist convection (Fig. 4e). The

suppressed convection then leads to a reduction in the detrainment of convective mass flux into the large-scale environment above 800 hPa (as can be seen from reduced water vapor by convection above 800 hPa in

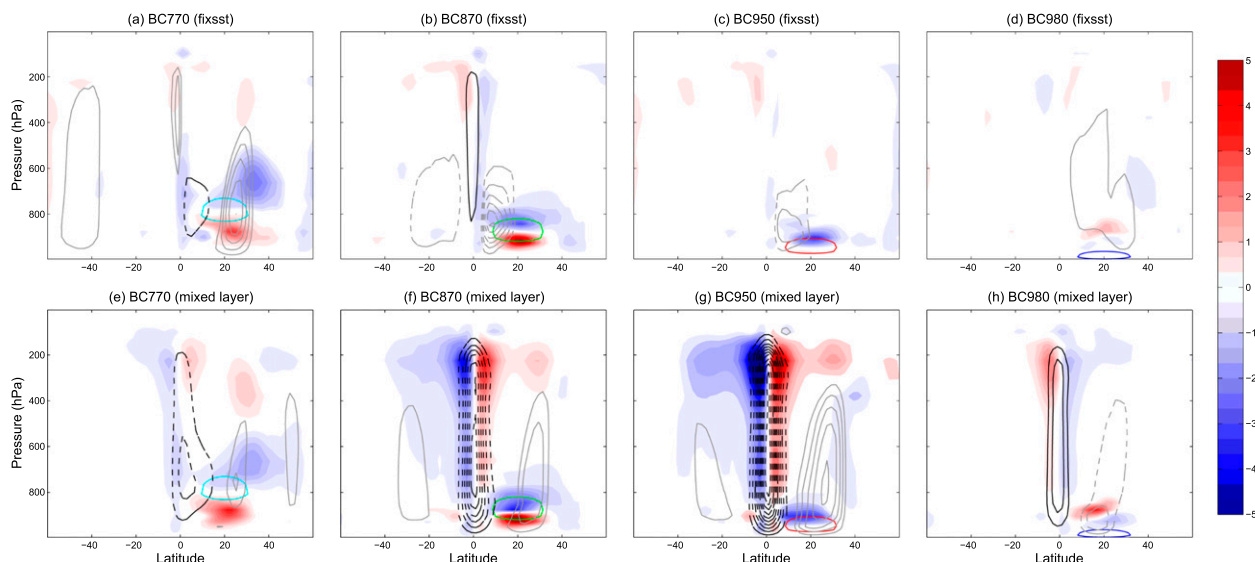


FIG. 5. Shading indicates the zonal-mean change in cloud amount (%). Contours indicate the zonal-mean change in mean meridional streamfunction. Dashed (solid) lines indicate the anomalous counterclockwise (clockwise) circulation and black (gray) color indicates the contour interval of  $9 \times 10^9$  ( $1.5 \times 10^9$ )  $\text{kg s}^{-1}$ . (top) From the fixed SST experiments and (bottom) the mixed layer experiments in (a),(e) BC770; (b),(f) BC870; (c),(g) BC950; and (d),(h) BC980.

Fig. 4c), lowering the cloud top and resulting in a reduction of clouds above the BC layer (Fig. 4f). Below 850 hPa, the relative humidity increases as convective mass is detrained at lower levels (Fig. 4d), and the resulting enhancement of large-scale condensation (Fig. 4c) substantially increases the cloud amount there (Fig. 4f). The cloud-bottom thickening outweighs the cloud-top thinning, leading to an overall increase in low cloud cover. The resulting increase in SW reflection (Fig. 3b) gives rise to a substantial TOA cooling (Fig. 3a) and the surface temperature drops by 0.5 K at 20°N (Fig. 1a) despite significant warming at 750–850 hPa from SW absorption by BC.

Cloud amount changes in BC870 can be explained in a similar manner, except for their larger magnitudes, which can be attributed to the vertical structure of the climatological cloud distribution that maximizes between 850 and 900 hPa. The cloud-top thinning slightly outweighs the cloud-bottom thickening to result in small positive  $\delta\text{CRF}$  (Fig. 3b). This amplifies the direct SW warming by BC, leading to surface warming in the northern subtropics (Fig. 1a).

In BC950, BC-induced SW heating is located near the cloud base (Fig. 4a). The maximum warming at 950 hPa (Fig. 4b) increases the saturated water vapor pressure and reduces the relative humidity (Fig. 4d), which gives rise to a substantial reduction of condensation at the cloud base (Fig. 4c). The resulting reduction in latent heat release suppresses the development of convective activity, as demonstrated by a reduction of convective

mass flux (Fig. 4e), leading to a substantial reduction in cloud amount (Fig. 4f). Also evident is a slight increase in cloud amount below 950 hPa because of increasing moisture in the boundary layer. The moister boundary layer can be attributed to 1) increased surface evaporation that is evenly distributed by turbulent diffusion and 2) a more stable boundary layer that limits the level of vertical diffusion to 950 hPa. A substantial reduction in low cloud cover gives rise to a significantly positive net TOA flux (Fig. 3a), leading to a large surface warming (Fig. 1a).

In BC980, the lowest model level gets warmer and everywhere above 950 hPa becomes cooler, making the low troposphere unstable (Fig. 4b). The low-level warming will increase the buoyancy of air parcels near the surface to enhance the strength of surface-based convection. However, the lifting condensation level (LCL) is raised because of a reduction in the relative humidity near the cloud base (Fig. 4d) that results from the low-level warming. Hence, the cloud amount decreases below 950 hPa, around the vertical level of the cloud base in the control experiment. Above 950 hPa, the cloud amount increases as the buoyancy of air parcels increases and enhances convection (Fig. 4e). The cloud-top thickening outweighs the cloud-bottom thinning, leading to an overall increase in low cloud cover and causing a significant reduction in net TOA flux (Fig. 3a), which results in surface cooling up to 0.5 K at 15°N (Fig. 1a).

A comparison of the top and bottom panels of Fig. 5 indicates that changes in the lower tropospheric cloud distribution in the northern subtropics are not strongly

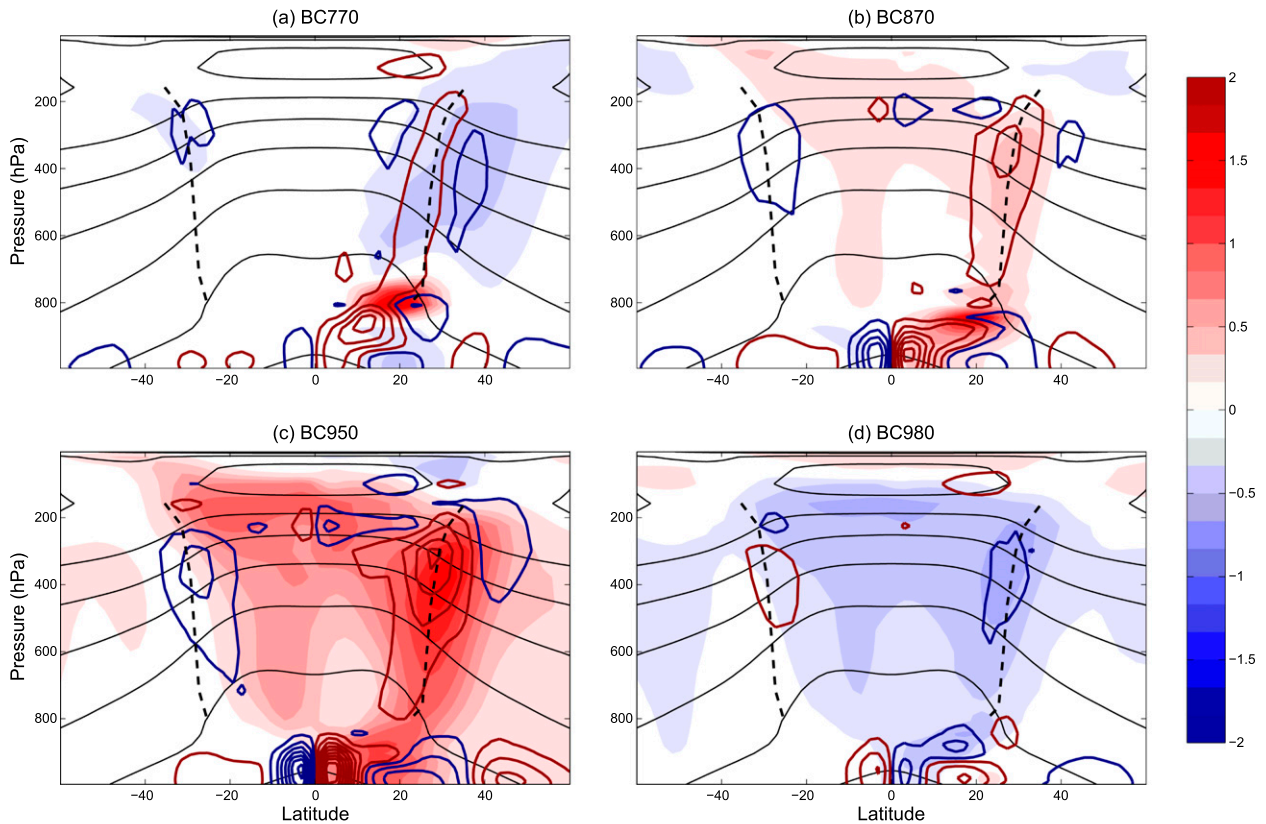


FIG. 6. Shading indicates the ensemble-mean zonal-mean change in temperature (K), and colored contours indicate the anomalous meridional temperature advection due to changes in meridional wind,  $-\delta\bar{v}(\partial\bar{T}_c/\partial y)$ , with positive values in brown and negative values in blue (the zero contour is omitted) in (a) BC770, (b) BC870, (c) BC950, and (d) BC980. Note that the values of the first positive and negative colored contours are both  $1 \times 10^{-7} \text{ K day}^{-1}$  in magnitude, with an interval of  $3 \times 10^{-7} \text{ K day}^{-1}$ . Black contours indicate the zonal-mean temperature in the control experiment ( $\bar{T}_c$ ; with an interval of 15 K and maximum value of 300 K near the surface) and black dashed lines indicate the latitude at which  $\partial\bar{T}_c/\partial y$  is maximum at each level.

affected by the SSTs. This implies that changes in these clouds are fast responses to local changes in atmospheric static stability and associated changes in convective mass flux, as described above. There still lacks a more coherent theory about what determines the relative importance of responses at cloud top and cloud bottom, but providing such general mechanism is beyond the scope of this study.

Overlaid as contours in Fig. 5 are changes in the mean meridional streamfunction  $\psi$  where

$$\psi(\varphi, p) = \frac{1}{g} \int_{p_0}^p \int_0^{2\pi} v a \cos\varphi d\lambda dp,$$

with  $v$  being the meridional wind and the other variables having their canonical definitions. In the mixed layer experiments, the two cases (BC870 and BC950) in which BC warms the northern subtropical atmospheric column (i.e., positive  $\delta R_{\text{TOA}}$  in Fig. 3a) exhibit a northward shift of the rising branch of the HC, with the opposite response in BC980, consistent with the ITCZ responses in Fig. 2b. In BC770, the northern subtropical surface is

cooled (Fig. 2a), but the meridional streamfunction is slanted northward toward an accentuated low-level atmospheric warming due to the direct SW absorption by BC (Fig. 5e), leading to a slight northward ITCZ shift (Fig. 2b). The ITCZ shift accompanies a shift in the cloud distribution in the equatorial region, as shown by the dipole pattern of changes in cloud fraction straddling the equator. A poleward transport by the upper branch of the HC results in changes in high clouds above 400 hPa in the subtropics. In contrast, in the fixed SST experiments, the ITCZ is bound to stay near the equator, so that the HC and high clouds in the subtropics barely change. This explains the differences in  $\delta\text{CRF}$  and  $\delta\text{CRF}_{\text{fixsst}}$  in Fig. 3. In addition to changes in the rising branch, the HC exhibits a clear shift in the descending branch in the northern subtropics. For example, in BC950, the northern subtropical static stability increases substantially (Fig. 6c), resulting from changes in the circulation (as explained in the next paragraph), and the northern HC exhibits a significant expansion (Fig. 5g) (Lu et al. 2007; Kang and Lu 2012).

These changes in large-scale circulation explain the robust horseshoe-shaped pattern in the vertical, zonal-average temperature response. Figure 6 shows the temperature response (shading) and the meridional temperature advection by changes in the mean meridional wind  $\delta\bar{v}$ , that is  $-\delta\bar{v}(\partial\bar{T}_c/\partial y)$  (colored contours), where  $\bar{T}_c$  is the mean temperature distribution in the control experiment (black contours). Note that the contribution to the anomalous meridional temperature advection above 800 hPa from changes in the temperature,  $-\bar{v}_c(\partial\delta\bar{T}/\partial y)$ , and the cross term is minimal (not shown). In all cases, warming is induced locally where BC is added, but in BC770 and BC980, cooling arises elsewhere because of the negative  $\delta\text{CRF}$ . The lower tropospheric temperature response in the northern subtropics is transported equatorward by the lower branch of the HC. Anomalous vertical motion in the equatorial region resulting from the ITCZ shift creates adiabatic temperature changes. This provides a reason for the weaker midtropospheric temperature response in the northern deep tropics. In the upper troposphere, the tropical temperature response is homogenized because of the weak temperature gradient criteria (Sobel et al. 2001). In the subtropics, the temperature response is slanted upward and poleward (or downward and equatorward). The consistency of the patterns of  $-\delta\bar{v}(\partial\bar{T}_c/\partial y)$  (colored contours) and temperature response (shading) indicates that the slanted subtropical temperature response is the result of  $\bar{T}_c$  being homogenized up to higher latitudes at upper levels, as demonstrated by the tilted line of maximum meridional temperature gradient (black dashed). The subtropical temperature response is larger in the Northern Hemisphere where the HC response is stronger (Fig. 5).

The zonal-mean temperature response exhibits a typical pattern of hemispherically asymmetric forcing akin to realistic aerosol distributions in CMIP5 climate simulations (see Fig. S4 in Xie et al. 2013). This similarity suggests the possibility of a robust climate response to radiative changes. It is worth highlighting that the sign of global temperature response is opposite in BC950 and BC980 despite only one model layer difference in the vertical level of prescribed BC. This implies that models must accurately capture the vertical distribution of BC to enhance the precision of simulating the climatic impact of BC.

#### 4. Summary and discussion

In this study, we investigate the sensitivity of the climate response to the altitude of BC using an atmospheric model coupled to an aquaplanet mixed layer

ocean. To represent a realistic geographical distribution of BC, it is added in the northern subtropics at different levels relative to the altitude of climatological subtropical low clouds. Our experiments are idealized in the sense that the effects of seasonality and land distribution are neglected and the BC distribution is highly idealized. However, the climatic impacts of BC are so uncertain that we believe such an idealized setup should precede more realistic simulations in order to first unveil fundamental mechanisms.

Consistent with many other studies, we show that clouds play an extremely important role in determining the climate responses to BC. The BC added below (950 hPa) or within (870 hPa) subtropical low clouds suppresses the development of convective activity, resulting in a reduction of low cloud amount to produce a positive cloud radiative forcing. The warmer northern subtropics then induce a northward shift of the ITCZ and a poleward extension of the descending branch of the northern Hadley cell. As the BC-induced local warming is amplified by clouds and is advected by the anomalous Hadley circulation, the entire globe gets warmer. In contrast, the BC added near the surface (980 hPa) increases the buoyancy of air parcels to enhance convection, which leads to an increase in the subtropical low cloud amount to produce a negative cloud radiative forcing. Hence, the temperature increases only locally where BC is added and decreases elsewhere. As a result, the ITCZ is shifted southward and the descending branch of the northern Hadley cell contracts equatorward. Despite the opposing signs of temperature and precipitation responses, the zonal-mean temperature response exhibits a robust horseshoe-shaped pattern in all cases. It is surprising that only one model layer difference in the level of prescribed BC creates completely opposite climate responses. Our results highlight the clear importance of computing vertical transport of BC with fidelity to enhance the skill of climate models in simulating the BC effects on climate.

The interaction between the semidirect effect and the indirect effect is highly uncertain (Hill and Dobbie 2008), so that the inclusion of the indirect effect may amplify or diminish the semidirect effect. Further study is required to assess the impact of indirect effect. In addition, large uncertainty in parameterization of convection and clouds (Stevens and Bony 2013) suggests the need for benchmark computations that can facilitate comparisons of the dependence of climate responses on the altitude of BC in a wide range of GCMs.

*Acknowledgments.* We thank Profs. Robert Wood, Rokjin J. Park, Shang Ping Xie, and Kelly McCusker for valuable discussions. We also thank Brian Rose and one

anonymous reviewer for their constructive comments that helped to improve an earlier version of the paper. S.M.K. is supported by the Basic Science Research Program through the National Research Foundation of Korea (NRF) funded by the Ministry of Science, ICT and Future Planning (2013R1A1A3004589). Y.T.H. is supported by the Ministry of Science and Technology of Taiwan through Grant 103-2111-M-002-013.

## REFERENCES

- Anderson, J. L., and Coauthors, 2004: The new GFDL global atmosphere and land model AM2-LM2: Evaluation with prescribed SST simulations. *J. Climate*, **17**, 4641–4673, doi:10.1175/JCLI-3223.1.
- Ban-Weiss, G. A., L. Cao, G. Bala, and K. Caldeira, 2012: Dependence of climate forcing and response on the altitude of black carbon aerosols. *Climate Dyn.*, **38**, 897–911, doi:10.1007/s00382-011-1052-y.
- Bond, T. C., D. G. Streets, K. F. Yarber, S. M. Nelson, J. Woo, and Z. Klimont, 2004: A technology-based global inventory of black and organic carbon emissions from combustion. *J. Geophys. Res.*, **109**, D14203, doi:10.1029/2003JD003697.
- , and Coauthors, 2013: Bounding the role of black carbon in the climate system: A scientific assessment. *J. Geophys. Res. Atmos.*, **118**, 5380–5552, doi:10.1002/jgrd.50171.
- Cook, J., and E. J. Highwood, 2004: Climate response to tropospheric absorbing aerosols in an intermediate general-circulation model. *Quart. J. Roy. Meteor. Soc.*, **130**, 175–191, doi:10.1256/qj.03.64.
- Feingold, G., H. L. Jiang, and J. Y. Harrington, 2005: On smoke suppression of clouds in Amazonia. *Geophys. Res. Lett.*, **32**, L02804, doi:10.1029/2004GL021369.
- Hansen, J., and Coauthors, 2005: Efficacy of climate forcings. *J. Geophys. Res.*, **110**, D18104, doi:10.1029/2005JD005776.
- Haywood, J. M., V. Ramaswamy, and B. J. Soden, 1999: Tropospheric aerosol climate forcing in clear-sky satellite observations over the oceans. *Science*, **283**, 1299–1303, doi:10.1126/science.283.5406.1299.
- Hill, A. A., and S. Dobbie, 2008: The impact of aerosols on non-precipitating marine stratocumulus. II: The semi-direct effect. *Quart. J. Roy. Meteor. Soc.*, **134**, 1155–1165, doi:10.1002/qj.277.
- Johnson, B. T., K. P. Shine, and P. M. Forster, 2004: The semi-direct aerosol effect: Impact of absorbing aerosols on marine stratocumulus. *Quart. J. Roy. Meteor. Soc.*, **130**, 1407–1422, doi:10.1256/qj.03.61.
- Kang, S. M., and J. Lu, 2012: Expansion of the Hadley cell under global warming: Winter versus summer. *J. Climate*, **25**, 8387–8393, doi:10.1175/JCLI-D-12-00323.1.
- , I. M. Held, D. M. W. Frierson, and M. Zhao, 2008: The response of the ITCZ to extratropical thermal forcing: Idealized slab-ocean experiments with a GCM. *J. Climate*, **21**, 3521–3532, doi:10.1175/2007JCLI2146.1.
- , D. M. W. Frierson, and I. M. Held, 2009: The tropical response to extratropical thermal forcing in an idealized GCM: The importance of radiative feedbacks and convective parameterization. *J. Atmos. Sci.*, **66**, 2812–2827, doi:10.1175/2009JAS2924.1.
- Koch, D., and A. D. Del Genio, 2010: Black carbon semi-direct effects on cloud cover: Review and synthesis. *Atmos. Chem. Phys. Discuss.*, **10**, 7685–7696, doi:10.5194/acp-10-7685-2010.
- Lu, J., G. A. Vecchi, and T. Reichler, 2007: Expansion of the Hadley cell under global warming. *Geophys. Res. Lett.*, **34**, L06805, doi:10.1029/2006GL028443.
- Ming, Y., V. Ramaswamy, P. A. Ginoux, and L. H. Horowitz, 2005: Direct radiative forcing of anthropogenic organic aerosol. *J. Geophys. Res.*, **110**, D20208, doi:10.1029/2004JD005573.
- , —, and G. Persad, 2010: Two opposing effects of absorbing aerosols on global-mean precipitation. *Geophys. Res. Lett.*, **37**, L13701, doi:10.1029/2010GL042895.
- Persad, G. G., Y. Ming, and V. Ramaswamy, 2012: Tropical tropospheric-only responses to absorbing aerosols. *J. Climate*, **25**, 2471–2480, doi:10.1175/JCLI-D-11-00122.1.
- Ramanathan, V., and G. Carmichael, 2008: Global and regional climate changes due to black carbon. *Nat. Geosci.*, **1**, 221–227, doi:10.1038/ngeo156.
- , P. J. Crutzen, J. T. Kiehl, and D. Rosenfeld, 2001: Aerosols, climate, and the hydrological cycle. *Science*, **294**, 2119–2124, doi:10.1126/science.1064034.
- , M. Ramana, G. Roberts, D. Kim, C. Corrigan, C. Chung, and D. Winker, 2007: Warming trends in Asia amplified by brown cloud solar absorption. *Nature*, **448**, 575–578, doi:10.1038/nature06019.
- Sakaeda, N., R. Wood, and P. J. Rasch, 2011: Direct and semidirect aerosol effects of southern African biomass burning aerosol. *J. Geophys. Res.*, **116**, D12205, doi:10.1029/2010JD015540.
- Sobel, A. H., J. Nilsson, and L. M. Polvani, 2001: The weak temperature gradient approximation and balanced tropical moisture waves. *J. Atmos. Sci.*, **58**, 3650–3655, doi:10.1175/1520-0469(2001)058<3650:TWTGAA>2.0.CO;2.
- Stevens, B., and S. Bony, 2013: What are climate models missing? *Science*, **340**, 1053–1054, doi:10.1126/science.1237554.
- UNEP/WMO, 2011: *Integrated Assessment of Black Carbon and Tropospheric Ozone: Summary for Decision Makers*. United Nations Environment Programme, 282 pp.
- Wang, C., 2013: Impact of anthropogenic absorbing aerosols on clouds and precipitation: A review of recent progresses. *Atmos. Res.*, **122**, 237–249, doi:10.1016/j.atmosres.2012.11.005.
- Xie, S. P., B. Lu, and B. Q. Xiang, 2013: Similar spatial patterns of climate responses to aerosol and greenhouse gas changes. *Nat. Geosci.*, **6**, 828–832, doi:10.1038/ngeo1931.
- Zarzycki, C. M., and T. C. Bond, 2010: How much can the vertical distribution of black carbon affect its global direct radiative forcing? *Geophys. Res. Lett.*, **37**, L20807, doi:10.1029/2010GL044555.
- Zelinka, M. D., and D. L. Hartmann, 2012: Climate feedbacks and their implications for poleward energy flux changes in a warming climate. *J. Climate*, **25**, 608–624, doi:10.1175/JCLI-D-11-00096.1.

Copyright of Journal of Climate is the property of American Meteorological Society and its content may not be copied or emailed to multiple sites or posted to a listserv without the copyright holder's express written permission. However, users may print, download, or email articles for individual use.